This article has been accepted for publication in a future issue of this journal, but has not been fully edited. Content may change prior to final publication. Citation information: DOI 10.1109/TMECH.2016.2557727, IEEE/ASME Transactions on Mechatronics

A Time Domain Approach to Control of Series Elastic Actuators: Adaptive Torque and Passivity-Based Impedance Control

Dylan P. Losey, *Student Member, IEEE*, Andrew Erwin, *Student Member, IEEE*, Craig G. McDonald, *Student Member, IEEE*, Fabrizio Sergi, *Member, IEEE*, and Marcia K. O'Malley, *Senior Member, IEEE*

***Abstract*— Robots are increasingly designed to physically interact with humans in unstructured environments, and as such must operate both accurately and safely. Leveraging compliant actuation, typically in the form of series elastic actuators (SEAs), can guarantee this required level of safety. To date, a number of frequency domain techniques have been proposed which yield effective SEA torque and impedance control; however, these methods are accompanied by undesirable stability constraints. In this paper, we instead focus on a time domain approach to the control of SEAs, and adapt two existing control techniques for SEA platforms. First, a model reference adaptive controller is developed which requires no prior knowledge of system parameters and can specify desired closed-loop torque characteristics. Second, the time domain passivity approach is modified to control desired impedances in a manner that temporarily allows the SEA to passively render impedances greater than the actuator's intrinsic stiffness. This approach also provides conditions for passivity when augmenting any stable SEA torque controller with an arbitrary impedance. The resultant techniques are experimentally validated on a custom prototype SEA.**

I. Introduction

As robots transition from factory floors to human environments, the importance of safety and torque control becomes increasingly paramount. Manipulators developed for surgical, rehabilitation, haptic, service, and other physically interactive applications must strive for the often contradictory goals of guaranteeing safety during contact while ensuring accurate, precise performance. Path planning, sensory feedback, and control strategies can all be used to mitigate unwanted torques perceived by the human user; however, these methods fail to reduce the severity of sudden impacts within unmodeled workspaces. On the other hand, physical compliance—elasticity between actuator and end-effector—offers a widely accepted means to fundamentally improve a manipulator's reflected dynamics, and is frequently incorporated in the design of inherently safe robots [1], [2]. Physical compliance is also well-suited for torque control because it converts input flows into output efforts, implicitly measures applied torques, and allows greater control gains than stiff manipulators [3].

Series elastic actuators (SEAs), originally introduced by [4], replace the traditionally rigid connection between transmission and load with an elastic component of non-adjustable stiffness. Advantages to series elastic actuators include increasing shock tolerance and lowering output impedance across the frequency spectrum—SEAs therefore provide desirable hardware platforms for human-robot interaction, especially in regards to rehabilitation devices [5], [6]. As such, a burgeoning body of research has been published concerning the control of SEAs; torque control [3], [7]–[16] and the effects of interaction schemes [17]–[20] have received particular attention. SEA torque control and interaction schemes have been predominately researched in the frequency domain [3], [7]–[11], [13]–[15], [17]–[20]. By contrast, this work alters time domain controller theories developed for rigid manipulators so they can be correspondingly applied within SEAs (see Fig. 1).

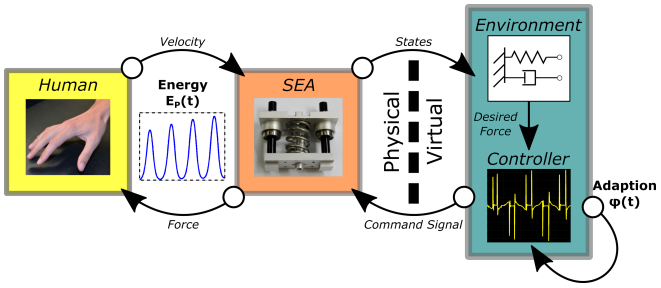

Fig. 1. Schematic of an SEA within an interaction control hierarchy. We propose using time domain functions, such as parameter adaption and interaction energy, to address both SEA torque or force control and the passivity of SEA impedance control.

SEA torque control, which can also be deemed actuator position control, strives to attain commanded spring displacements. Motor trajectories here don't directly determine the robot's path, but alternatively regulate the effort applied to contacting objects over time. Work by Pratt *et al*. [7] and Wyeth [8] demonstrated the effectiveness of cascaded torque control with an inner velocity loop and PI controllers. This linear scheme—among the most prevalent in the SEA literature—can be simply implemented using the conditions developed within [9], and offers a valuable platform for passivity analysis. Tuning is straightforward since theoretical closed-loop performance improves with increases in PI controller magnitude, but controller gains are practically limited by saturation, noise, and instability induced by discretization.

Subsequent research has attempted to outperform cascaded torque-velocity control via more advanced techniques. Robust

This work was supported in part by the NSF GRFP-0940902, by the NSF IGERT-1250104, and by the NSF CNS-1135916.

The authors are with the Mechatronics and Haptic Interfaces Laboratory, Department of Mechanical Engineering, Rice University, Houston, TX 77005. Fabrizio Sergi is now with the Department of Biomedical Engineering, University of Delaware, Newark, DE 19716. (e-mail: dlosey@rice.edu)

This article has been accepted for publication in a future issue of this journal, but has not been fully edited. Content may change prior to final publication. Citation information: DOI 10.1109/TMECH.2016.2557727, IEEE/ASME Transactions on Mechatronics

[10], [11], nonlinear [12], and optimal [13]–[15] control approaches have all been leveraged; theory and implementation demonstrate that each method can better eliminate disturbances than do cascaded torque-velocity controllers. Gains in performance, however, have generally increased controller complexity and added potential sources for instability. Applying the small-gain theorem, the stability of robust schemes can be shown to depend upon the magnitude of modeling errors. Nonlinear control introduces a trade-off between chattering and approximation, neither of which is desirable. The proposed optimal control techniques are "optimal" only in the sense of nominal models—errors increase with modeling uncertainty. Summarily, performance and knowledge have been directly correlated: to obtain better, stable results, more thorough identification experiments must be conducted.

Adaptive control, which promises the ability to safely dictate closed-loop torque control characteristics without requiring knowledge of system parameters, resolves this conflict. A modified model reference adaptive controller (MRAC) has recently been implemented on flexible joint manipulators [21], where it addressed modeling errors and parameter uncertainties while offering stability guarantees [22]. Calanca *et al*. [16] similarly developed a modified MRAC specifically for SEAs coupled to human operators; although their approach provides ultimately bounded stability when human behavior matches a simplified model, stability cannot be proven if the given dynamic equations are incomplete. In this paper, we instead derive an MRAC for SEAs which relies upon known manipulator dynamics without modeling human interaction, yet still specifies closed-loop characteristics. We will demonstrate both that the proposed MRAC drives the SEA to behave like some desired model—despite unknown parameters—and that this behavior is achieved with Lyapunov stability.

Once a method for obtaining desired torques is selected, subsequent steps often involve regulating the effort/flow exchange between user and SEA; this enables the SEA to display virtual environments, and provides structure to human-robot interaction. Vallery *et al*. [17] concluded that when SEAs render a pure stiffness with cascaded torque-velocity control, passivity can only be assured if the desired stiffness is less than or equal to the spring's actual stiffness. Tagliamonte and Accoto [18] extended Vallery's result, evaluating passivity when displaying series and parallel spring-damper systems by means of cascaded torque-velocity control. Mosadeghzad *et al*. [19] compared impedance schemes with inner velocity, torque, or position control loops. Finally, previous work from our lab [20] demonstrated that lead-lag compensators in conjunction with cascaded torque-velocity control could be leveraged to render stiffnesses greater than the spring stiffness; however, this non-passive behavior is only achieved with coupled stability for certain environments.

Thus far, studies of SEA interaction passivity have been restricted to linear torque controllers and limited impedance ranges. Accordingly, we here develop an impedance control method—inspired by the time domain passivity approach [23]—where energy measurements are utilized to overcome these restrictions. Ferraguti *et al*. [24] recently introduced an energy tank-based method in order to render fluctuating stiffnesses with rigid manipulators; analogously, when the energy stored by an SEA exceeds some threshold, we seek to adjust the virtual environment and display non-passive desired impedances. In this paper, we show that our proposed impedance passivity controller both regulates SEA interactions while maintaining at least input-to-state stability, and also safely enables previously inaccessible combinations of torque controllers and desired impedances.

This work reformulates time domain techniques for SEA torque and impedance control. In Section II we derive an MRAC for SEAs which estimates system parameters, specifies closed-loop behavior, and favorably compares with state-of-the-art techniques. We then utilize network theory in Section III to evaluate the stability of impedance control schemes, and describe an energy method which can be used to determine the passivity of any SEA torque controller in conjunction with an arbitrary virtual environment. We also propose a novel impedance controller which temporarily allows the SEA to passively render impedances greater than its intrinsic stiffness. Finally, in Section IV we experimentally validate both the adaptive torque controller and impedance passivity controller using an SEA prototype.

II. Adaptive Torque Control of SEAs

As explained by [3] and depicted in Fig. 2, the reduced second order model of an electromagnetic motor and transmission in series with a torsional spring is given by

$$\begin{aligned} \tau_L &= K(\theta_A - \theta_L) \\ \ddot{\theta}_A &= -\frac{B_A}{J_A}\dot{\theta}_A - \frac{1}{J_A}\tau_L + \frac{1}{J_A}\tau_A \end{aligned} \tag{1}$$

Or, re-written with Laplace variables

$$\theta_A = \frac{\tau_A + K\theta_L}{J_A s^2 + B_A s + K} \tag{2}$$

where J_A is the actuator inertia, B_A is the actuator damping, K is the torsional spring constant, θ_A is the actuator position, τ_A is the actuator torque, θ_L is the load position, and τ_L is the load torque. When the spring constant is known, sensing actuator and load positions implicitly measures the load torque.

Throughout this work we will assume that the above model completely describes SEA plant behavior. This requires the motor to be linear, and potentially ignores the effects of nonlinear friction, backlash, or saturation terms. We will also assume that motor and load velocities can be obtained without

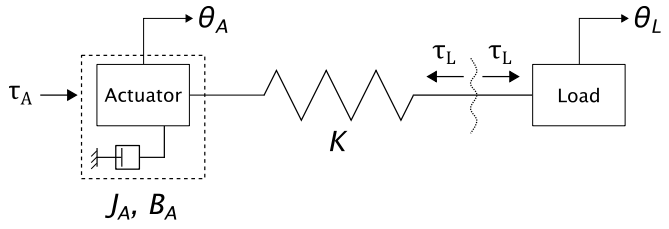

Fig. 2. Schematic of an SEA. Torques applied at the actuator affect spring displacement, which in turn both measures and determines load torques. The actuator, which may include the motor and transmission, is modeled as an inertia with driving torques and viscous damping.

This article has been accepted for publication in a future issue of this journal, but has not been fully edited. Content may change prior to final publication. Citation information: DOI 10.1109/TMECH.2016.2557727, IEEE/ASME Transactions on Mechatronics

significant time delay; this assumption is fairly common within SEA control, and may be alleviated by employing observers and/or filters operating at a much higher frequency than the physical system. The limitations of these assumptions—and their impacts on system stability—will be addressed in following sections. Although we will focus on rotary systems, our analysis can also be applied to translational configurations. Hence, references to SEA torque and force control should be regarded as interchangeable.

When designing a torque-controlled SEA for haptic applications, ideal closed-loop relationships are given by

$$\frac{\tau_L(s)}{\tau_{L,d}(s)} = 1, \quad \frac{\tau_L(s)}{\theta_L(s)} = 0 \tag{3}$$

where $\tau_{L,d}$ is the desired load torque. Noting that the spring element converts this torque control problem into a position control problem, we may analogously state

$$\frac{\theta_A(s)}{\theta_{A,d}(s)} = 1, \quad \frac{\theta_A(s)}{\theta_L(s)} = 0 \tag{4}$$

where $\theta_{A,d}$ is the desired actuator position corresponding to a desired load torque. In essence, controllers should strive (a) to quickly achieve a desired actuator position with minimal steady-state error, and (b) to decouple actuator and load positions as much as possible.

A. MRAC for SEA Torque Control

Several SEA torque controllers have been recently proposed which better achieve the aforementioned goals than do traditional cascaded torque-velocity controllers [10]–[15]; however, these new approaches also require accurate identification of system parameters. In order to both provide desired performance and autonomously identify system parameters, we here introduce a model reference adaptive controller (MRAC) for SEA torque control. Our derivation of an MRAC follows the overview presented in [25], and applies this well-established control theory to SEA mechanisms. MRAC—an adaptive servo system—selects parameters such that the plant tracks a reference model, which in turn provides the desired response to an input signal (see Fig. 3). In Section III we will describe an additional algorithm to ensure this MRAC maintains stability when coupled to any passive system via impedance control.

The open-loop SEA plant described by (1) can be rearranged in the following state space form

$$\begin{bmatrix}\dot{\theta}_A \\ \ddot{\theta}_A\end{bmatrix} = \begin{bmatrix}0 & 1 \\ -\frac{K}{J_A} & -\frac{B_A}{J_A}\end{bmatrix}\begin{bmatrix}\theta_A \\ \dot{\theta}_A\end{bmatrix} + \begin{bmatrix}0 \\ \frac{1}{J_A}\end{bmatrix}\Big(\tau_A - \mu_1 f_1(\dot{\theta}_A) - \mu_2 f_2(\dot{\theta}_A) + K\theta_L\Big)$$

$$\dot{X} = AX + B(\tau_A - \mu_1 f_1(\dot{\theta}_A) - \mu_2 f_2(\dot{\theta}_A) + K\theta_L) \tag{5}$$

where the states (X) and exogenous input (θ_L) are known; actuator and load positions are of course necessarily measured in SEAs, and we have already listed the assumption that their derivatives can be quickly obtained. In order to better account for any asymmetric Coulomb friction, we have added terms $\mu_1 f_1$ and $\mu_2 f_2$, where μ_1 and μ_2 are the Coulomb friction parameters. Nonlinear functions f_1 and f_2 approximate the sign of actuator velocity while maintaining continuity at $\dot{\theta}_A = 0$ via hyperbolic tangents.

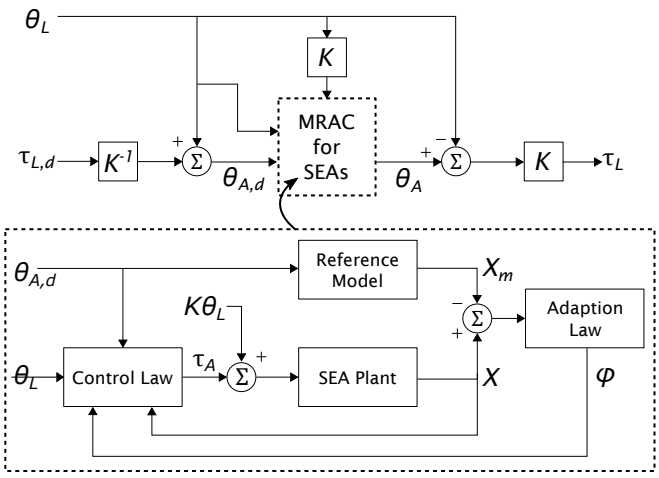

Fig. 3. Block diagram of our MRAC for SEA torque control. Desired load torques are first converted into desired actuator positions, $\theta_{A,d}$, which then become command signals for the MRAC. The torque resulting from load position ($K\theta_L$) serves as a known disturbance; the MRAC attempts to reject this disturbance with a feed-forward term. Using measured states and parameters identified by integrating the adaption law, the control law generates a signal which drives the plant to behave like a reference model. Note that θ_A, the ultimate output of the MRAC subsystem, can be simply extracted from X, the SEA state vector.

We next choose the desired closed-loop response to be a generic 2nd order transfer function, noting that this reference model is analogous to the feed-forward terms in [10] and [11]

$$\begin{bmatrix}\dot{\theta}_{A,m} \\ \ddot{\theta}_{A,m}\end{bmatrix} = \begin{bmatrix}0 & 1 \\ -\omega_n^2 & -2\zeta\omega_n\end{bmatrix}\begin{bmatrix}\theta_{A,m} \\ \dot{\theta}_{A,m}\end{bmatrix} + \begin{bmatrix}0 \\ \omega_n^2\end{bmatrix}\theta_{A,d}(t)$$

$$\dot{X}_m = A_m X_m + B_m \theta_{A,d} \tag{6}$$

Here $\theta_{A,d}$ is the command signal, and subscript m indicates "model." The natural frequency (ω_n) and damping ratio (ζ) should be picked to correspond with desired closed-loop poles and bandwidth; it is possible that these criteria will change depending on the assigned task. This form implies $\theta_{A,m}(s) \approx \theta_{A,d}(s)$ over sufficiently low frequencies, while exclusion of θ_L from the reference model decouples actuator and load position—hence, the given reference model can be tuned to meet our SEA performance objectives. We will assume that users select a stable A_m.

A control law with which it is possible to make the open-loop system behave like the closed-loop reference model is given by

$$\tau_A = -LX + M\theta_{A,d} + \hat{\mu}_1 f_1(\dot{\theta}_A) + \hat{\mu}_2 f_2(\dot{\theta}_A) - \hat{K}\theta_L \tag{7}$$

where L and M contain the estimated inertia, viscous damping, and stiffness such that

$$L = \begin{bmatrix}L_1, & L_2\end{bmatrix} = \begin{bmatrix}\hat{J}_A\omega_n^2 - \hat{K}, & 2\hat{J}_A\zeta\omega_n - \hat{B}_A\end{bmatrix}$$
$$M = \hat{J}_A\omega_n^2 \tag{8}$$

We note that L and M specify $\hat{J}_A$, $\hat{B}_A$, and $\hat{K}$, and that $\hat{K}$ can be extracted from (8) using $\hat{K} = M - L_1$. Substituting

This article has been accepted for publication in a future issue of this journal, but has not been fully edited. Content may change prior to final publication. Citation information: DOI 10.1109/TMECH.2016.2557727, IEEE/ASME Transactions on Mechatronics

this control law (7) into our SEA plant (5), the closed-loop system then becomes

$$\dot{X} = (A - BL)X + BM\theta_{A,d} + BY \tag{9}$$
$$Y = (\hat{\mu}_1 - \mu_1)f_1(\dot{\theta}_A) + (\hat{\mu}_2 - \mu_2)f_2(\dot{\theta}_A) - (\hat{K} - K)\theta_L$$

Consider an idealized case where $Y = 0$ due to perfect estimation of μ_1, μ_2, and K. Since the columns of $A - A_m$ and B_m are linear combinations of the vector B, there exist some "true" parameter values L^* and M^* for which (9) equals (6); i.e., $A_m = A - BL^*$ and $B_m = BM^*$. As such, the proposed control law can yield accurate tracking of the reference model.

Let error between the plant and model states be defined as $e = X - X_m$. Taking the derivative of e before plugging in (9) and (6), we arrive at

$$\dot{e} = -A_m X_m + (A - BL)X + (BM - B_m)\theta_{A,d} + BY \tag{10}$$

By adding and subtracting $A_m X$, the above expression can be more conveniently rearranged as

$$\dot{e} = A_m e + (A - BL - A_m)X + (BM - B_m)\theta_{A,d} + BY \tag{11}$$

Recall that Y is linearly parameterizable; given the existence of L^* and M^*, the second and third terms in (11) are likewise parametrized to $B(-X^T)(L - L^*)^T$ and $B\theta_{A,d}(M - M^*)$. Accordingly,

$$\dot{e} = A_m e + \Psi(\phi - \phi^*) \tag{12}$$
$$\Psi = B\begin{bmatrix} -\theta_A + \theta_L & -\dot{\theta}_A & \theta_{A,d} - \theta_L & f_1(\dot{\theta}_A) & f_2(\dot{\theta}_A) \end{bmatrix}$$

where Ψ is the regressor matrix, $\phi = (L, M, \hat{\mu}_1, \hat{\mu}_2)^T$, and superscript * still denotes "true" parameter values. We here utilized the dependence of $\hat{K}$ on M and L_1 to maintain the dimensionality of the parameter space. During implementation, J_A, and therefore B, are unknown—however, using a scaled $\hat{B} = cB$ affects adaption rates but does not alter stability. Stable error dynamics $\dot{e} = A_m e$ are obtained if $\phi = \phi^*$.

In order to derive the parameter adaption law, we propose a Lyapunov candidate function that minimizes error magnitude subject to the constraint condition $\phi = \phi^*$

$$V(t) = \frac{1}{2}\gamma e^T P e + \frac{1}{2}(\phi - \phi^*)^T(\phi - \phi^*) \tag{13}$$

P is symmetric positive definite, and a corresponding symmetric positive definite Q can be found per the Lyapunov equation and Kalman-Yakubovich lemma [25]. Scalar γ is a weighting term that influences the speed with which (13) converges, or, correspondingly, the rate of parameter adaption. The time derivative of V is given by

$$\dot{V}(t) = \frac{1}{2}\gamma e^T P\big(A_m e + \Psi(\phi - \phi^*)\big) + \frac{1}{2}\gamma\big(e^T A_m^T + (\phi - \phi^*)^T\Psi^T\big)Pe + (\phi - \phi^*)^T\dot{\phi} \tag{14}$$

where $\dot{e}$ has been replaced by (12). Manipulating this equation, we obtain

$$\dot{V}(t) = \frac{1}{2}\gamma e^T(A_m^T P + PA_m)e + \gamma(\phi - \phi^*)^T\Psi^T Pe + (\phi - \phi^*)^T\dot{\phi} \tag{15}$$

Now applying Q, whose existence is here guaranteed by the Lyapunov equation, the time derivative of V becomes

$$\dot{V}(t) = -\frac{1}{2}\gamma e^T Q e + (\phi - \phi^*)^T\big[\dot{\phi} + \gamma\Psi^T Pe\big] \tag{16}$$

With the archetypal parameter adaption law

$$\dot{\phi} = -\gamma\Psi^T Pe \tag{17}$$

$\dot{V}$ is negative semi-definite, and hence the closed-loop system is Lyapunov stable. Recognizing both that $e \in L_2$ and $\dot{e}$ is bounded, we can apply Barbalat's Lemma to prove $e(t) \to 0$ as $t \to \infty$. We therefore conclude that the proposed control (7) and adaption (17) laws provide a stable MRAC which can be used to drive the open-loop SEA plant (5) to behave like some desired closed-loop reference model (6). No prior parameter identification is necessary so long as the SEA can be described with (5); rather, estimates of J_A, B_A, K, μ_1, and μ_2 are iteratively updated by our parameter adaption law.

Consider an ideal case where the plant's closed-loop response is dictated by the MRAC reference model (i.e., $e = 0$). Since the reference model (6) is a low-pass filter in the Laplace domain, $Q_f(s)$, we can write $\theta_A = Q_f(s)\theta_{A,d}$. Substituting this expression into (1), we find

$$\tau_L = K\big(Q_f(s)\theta_{A,d} - \theta_L\big) \tag{18}$$

Relating desired actuator positions and desired load torques, i.e., $\theta_{A,d} = K^{-1}\tau_{L,d} + \theta_L$, it can be shown that

$$\tau_L = Q_f(s)\tau_{L,d} + K\big(Q_f(s) - 1\big)\theta_L \tag{19}$$

A cursory examination of the frequency response $\tau_L(j\omega)$ complements both our intuition and the objectives outlined in (3). As the frequency decreases, $Q_f(j\omega) \to 1$, and the desired torque is realized with minimal impedance. On the other hand, as the frequency increases, $Q_f(j\omega) \to 0$, and the impedance approaches the physical spring's stiffness. Use of the final value theorem further demonstrates that step changes in load position do not initiate steady-state errors in load torque.

Although state error convergence is a property of the controller, parameter estimation error is largely determined by the input signal. Because $\dot{V}$ is bounded, $\phi - \phi^*$ is also bounded; if certain input conditions are met—such as persistent excitation—then $\phi \to \phi^*$ as $t \to \infty$, and plant parameters can be accurately estimated. Fortunately, parameter estimation is here of secondary importance—we are unconcerned by how "correct" the parameters are, so long as the controller functions satisfactorily.

B. Comparison of Adaptive and Robust SEA Torque Control

We have thus far assumed that the linear model in (1) describes our SEA plant. Now we relax that assumption and consider the effects of model variation, which can be interpreted as an unknown multiplicative perturbation Δ. If we rewrite the open-loop SEA plant as

$$\theta_A = \frac{\tau_A + K\theta_L}{J_A s^2 + B_a s + K}\big(1 + \Delta(s)\big) \tag{20}$$

This article has been accepted for publication in a future issue of this journal, but has not been fully edited. Content may change prior to final publication. Citation information: DOI 10.1109/TMECH.2016.2557727, IEEE/ASME Transactions on Mechatronics

a constraint guaranteeing stability of the closed-loop plant is given by

$$\left|\frac{J_A s^2 + (L_2^* + B_A)s + (L_1^* + K)}{L_2^* s + L_1^*}\right| > |\Delta(s)| \qquad (21)$$

L_1 and L_2, originally defined in (8), are parameters directly associated with the difference between A, the plant dynamics, and A_m, the reference model dynamics, via the equation $A_m = A - BL^*$. Reference models similar to the actual plant are therefore more robust to unmodeled behavior; generally, the magnitude of Δ should be less than one over a relevant frequency range. As explained in [26], Δ also introduces an additional term to the error equation (12)—which in the worst case induces instability via unbounded adaption parameter drift, and in the best case causes small tracking errors and bounded adaption parameters. Without precise knowledge of Δ, however, stability and global adaption parameter boundedness cannot be evaluated [26].

While our adaption law effectively makes system stability more susceptible to unmodeled behavior, we selected an adaptive controller because the principal sources of unmodeled behavior are here largely eliminated. Since the MRAC determines plant parameters and spring deflection measures external disturbances, Δ arises purely from unmodeled motor dynamics. Use of adaptive control therefore transforms the parameter estimation problem into a modeling problem; this is advantageous because (a) DC motor dynamics are well studied and (b) each model applies to a larger class of devices than would a specific parameter set.

The proposed adaptive controller strongly resembles robust controller methods presented in [10] and [11]. MRAC desired closed-loop response is given by a reference model—for DOB control, the desired closed-loop response is given by a feed-forward filter. Our unmodeled behavior stems solely from unmodeled dynamics, while robust plant uncertainties incorporate parameter and modeling errors. Finally, neither controller can guarantee stability without explicitly knowing Δ—although DOBs by and large provide stronger stability assurances than MRACs. We conclude that the tradeoff between these SEA control approaches revolves around model accuracy; in cases where the stated dynamics roughly apply, the outlined MRAC offers similar performance and stability with no prerequisite parameter knowledge. We experimentally demonstrate in Section IV that parameter uncertainty does not alter MRAC long-term performance, but can destabilize comparable DOB methods. Practically, it may be logical to first test an adaptive approach before investing time in the identification experiments requisite for robust controllers.

III. Passive Impedance Control of SEAs

Impedance control—as explained by Hogan [27]—regulates interactions between robot and environment by specifying the relationship between input flow and output effort. Let the impedance control law be defined as

$$\tau_{L,d} = Z_d(\dot{\theta}_{L,d} - \dot{\theta}_L) \qquad (22)$$

where Z_d is the desired impedance and $\theta_{L,d}$ is the reference path; generalized output torques $\tau = \{\tau_{L,d},\ \tau_L\}$ are accordingly functions of both $\dot{\theta}_{L,d}$ and $-\dot{\theta}_L$. To differentiate between torques stemming from the task trajectory and those caused by environmental interaction, we will indicate torques which result purely from $-\dot{\theta}_L$ as

$$\tau' = \tau - \tau_{ref} \qquad (23)$$

Here τ_{ref}, a known quantity which can be determined from the controller and/or plant, represents output torques as a function of the reference path. Under this notation, an SEA's impedance transfer function defines the relationship between input velocity $-\dot{\theta}_L$ and corresponding output torque τ'_L.

Since impedance shapes energy exchanges, passivity is frequently used to evaluate impedance controller stability [28]. Loosely speaking, a system is passive if it dissipates or conserves energy; i.e., the quantity of released energy must be less than or equal to the amount of supplied energy. An interconnected system of passive networks is necessarily passive—the concept of passivity therefore allows us to conclude global stability by assessing each constituent's energy exchange. If a robot is known to be passive, coupling that robot with any passive environment—such as a passive human operator—results in stable interaction, and does not require extensive modeling or parameterization of the environment.

A. SEA Impedance Control

Impedance control and passivity have recieved particular attention in relation to SEAs [17]–[20]. Prior research has focused on cascaded torque controllers, in part because the passivity of linear time-invariant systems can be straightforwardly tested. Should the impedance transfer function be positive real (PR), the amount of dissipated energy must be greater than or equal to zero; evaluating the positive realness of impedance therefore offers a frequency domain determination of device passivity. Consider, for example, an idealized impedance transfer function obtained by combining (19) and (22)

$$Z(s) = \frac{\tau'_L}{-\theta_L s} = \frac{K + \big(Z_d(s)s - K\big)Q_f(s)}{s} \qquad (24)$$

Given a stable transfer function $G(s) = A(s)/B(s)$ whose poles upon the imaginary axis are simple, $G(s)$ is PR if and only if its real part is nonnegative along the $j\omega$ axis. One check for this criterion follows from the equation

$$Re\big(G(j\omega)\big) = Re\frac{A(j\omega)}{B(j\omega)} = Re\frac{A(j\omega)B(-j\omega)}{B(j\omega)B(-j\omega)} \qquad (25)$$

so at frequencies where $Re\big(A(j\omega)B(-j\omega)\big) \geq 0$, we can conclude $G(s)$ is PR. Applying this test to (24) and letting $Z_d s = K_d$, we again find $K_d \leq K$ to be the requisite condition for passivity. The range of virtual impedances is thus limited even for a best-case controller—restrictions ultimately stem from mechanical time delays induced by the spring, but may differ amongst controllers.

Although the described PR property can evaluate linear controller passivity, this method (a) requires each desired

This article has been accepted for publication in a future issue of this journal, but has not been fully edited. Content may change prior to final publication. Citation information: DOI 10.1109/TMECH.2016.2557727, IEEE/ASME Transactions on Mechatronics

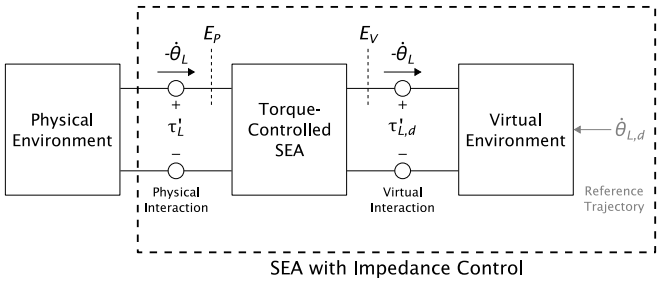

Fig. 4. Network model of an SEA with impedance control. The two-port torque-controlled SEA is terminated by passive environments, and energies at these connecting ports can be calculated from the corresponding effort/flow pairs. The reference trajectory—and its effect on output torques—is omitted in order to purely study interaction energies. Note that while the "torque-controlled SEA" block could refer to the method depicted in Fig. 3, other torque control approaches, such as those presented in [8] or [10], may also be implemented here.

class of impedances to be individually examined and (b) cannot be simply used by time-variant controllers. In order to determine the passivity of any stable SEA torque controller in conjunction with an arbitrary desired impedance, we introduce the time domain passivity approach (TDPA) for SEAs. The TDPA is less conservative than comparable frequency domain tests; a signal non-passive over any frequency range may be output passively during certain time-spans. Indeed, we will find that the described TDPA enables temporarily rendering virtual stiffnesses above the plant's natural stiffness—relaxing conditions established by the literature [17]–[20].

B. Energy Analysis Using TDPA

An SEA interface with impedance control can be interpreted as interconnected one- and two-port networks: physical environment, torque-controlled plant, and affixed virtual environment (see Fig. 4). Users move the SEA end-effector with some velocity $\dot{\theta}_L$ that is measured in the plant and transmitted to the virtual environment; the virtual environment specifies a corresponding torque $\tau'_{L,d}$ which is returned to the torque-controlled plant—and, after a time delay, τ'_L is finally output to the user. Network theory has been extensively applied to examine energy flows through rigid haptic interfaces [29] as well as during bilateral teleoperation [30], a related topic within the field of human-robot interaction.

Viewed across the lenses of network theory, the total energy of a system is equivalent to the sum of the energies supplied by each port plus the network's initial energy; for the sake of simplicity, however, we will omit this initial term. The energy of an SEA torque-controlled plant is thus written

$$E(t) = E_P(t) - E_V(t) \tag{26}$$

where energy across physical (E_P) and virtual (E_V) interaction ports is given by

$$E_P(t) = \int_0^t \tau'_L(\lambda)\big(-\dot{\theta}_L(\lambda)\big)d\lambda \tag{27}$$

$$E_V(t) = \int_0^t \tau'_{L,d}(\lambda)\big(-\dot{\theta}_L(\lambda)\big)d\lambda \tag{28}$$

Recalling fundamental assumptions of both physical and virtual environment passivity, our SEA network is guaranteed passive if the two-port torque-controlled plant is also passive—i.e., $E(t) \geq 0\ \forall t$. One safe criteria for passivity is $\tau'_L(t) \geq \tau'_{L,d}(t)\ \forall t$, or $Z(s) \geq Z_d(s)\ \forall s$ in the frequency domain; since $Z(s)s \to K$ as $s \to \infty$, we may alternatively write $K \geq Z_d(s)s$ as the requisite condition for energy dissipation. The passivity of any desired impedance and stable torque controller can therefore be confirmed by iteratively measuring (27) and (28)—and, at times when $E_P < E_V$, altering $\tau'_{L,d}$ to satisfy the listed inequalities.

With an aim to instrument and dissipate energy in the time domain, Hannaford and Ryu [23] developed passivity observers (POs) and passivity controllers (PCs). These techniques assume both that effort and flow variables are sampled at a much faster rate than the system dynamics, and that torque and velocity fluctuations between testing periods are slight; as such, they are suited to SEA applications where θ_L changes continuously over low frequencies. POs consist of a discrete-time implementation of the energy equation at relevant ports—PCs are time-varying dampers selected to impose a lower bound on energy. By means of POs and PCs we can modify $\tau'_{L,d}$ such that (26) is always nonnegative, yielding a simple yet versatile assurance of SEA passivity.

We have described how the TDPA can be utilized to ensure SEA torque controllers are passive; however, this condition is unnecessarily strict. The amount of stored or released energy within an arbitrarily connected network system is determined by effort and flow variables at each open-ended port [23]. Passivity of an entire SEA robot—torque-controlled plant and virtual environment—can therefore be evaluated using only E_P; individual blocks need not be dissipative so long as the network system is passive with respect to the physical interaction port. Incidentally, determining passivity by measuring E_P provides the time domain corollary to the previously mentioned frequency domain PR tests.

C. TDPA for SEAs

A coupled SEA plant, torque controller, and impedance controller are passive with respect to environmental interactions at time t if and only if $E_P(t)$ is nonnegative. Given that spring displacement measures τ_L, the controllers dictate τ_{ref}, and filtered differentiation obtains $\dot{\theta}_L$ with negligible delays, E_P can be observed in real time by implementing (27). Our assumption that τ_{ref} is known requires plant parameterization; however, this information was already necessary to construct the torque controllers enumerated in Section II, and the following algorithm includes a safety factor which accounts for τ'_L errors. Bearing in mind the TDPA previously presented, it seems τ'_L can be similarly adjusted to guarantee E_P passivity.

Unfortunately, changing load torque entails shifting actuator position. Rearranging (1)

$$\tau_L = \frac{\tau_A - (J_A s^2 + B_A s)\theta_L}{\frac{J_A}{K}s^2 + \frac{B_A}{K}s + 1} \tag{29}$$

it is evident that decreasing K increases a mechanical time delay between actuator and load torques. The compliant element

This article has been accepted for publication in a future issue of this journal, but has not been fully edited. Content may change prior to final publication. Citation information: DOI 10.1109/TMECH.2016.2557727, IEEE/ASME Transactions on Mechatronics

therefore prevents us from treating SEA motors as transparent effort sources; this contrasts the rigid haptic manipulators studied by [23], [24], offers challenges dissimilar to communication time delays, and prohibits the straightforward use of a PC. Since τ_A can be instantaneously varied and the plant (29) is passive, a secondary solution involves directly modulating the commanded controller torque to maintain interaction passivity. Yet mechanical time delays again disrupt the suggested plan—present actuator torques have an effect on future load torques, and hence upcoming input velocities would be required to evaluate current torque selection. Moreover, discontinuously switching the controller signal may excite spring oscillations and nonintuitively affect load torques.

In order to promise passivity despite mechanical time delays, we here introduce an impedance passivity controller (iPC) which autonomously adjusts the desired impedance based on physical interaction energy. When E_P approaches zero, the iPC should alter Z_d such that the SEA dissipates energy; on the other hand, when E_P is above some threshold, our iPC ought to faithfully output the desired impedance. This algorithm, analogous to that used in [24], is formalized below

$$Z_d' = Z_d + f(E_P)(Z_d^* - Z_d)$$
$$f(E_P) = \begin{cases} 0 & \text{if } E_P \geq E_U \\ 1 & \text{if } E_P \leq E_L \\ \frac{E_U - E_P}{E_U - E_L} & \text{otherwise} \end{cases} \tag{30}$$

where E_L and E_U define the lower and upper limits of the interpolation region, and Z_d^* is a predefined impedance such that $Z \geq Z_d^*$. If $E_P \leq E_L$, the iPC renders Z_d^*, and thereby imposes a nondecreasing lower bound on physical interaction energy. Accordingly, energy generated by an SEA with the proposed iPC is necessarily bounded by some finite value: $E_P \geq -\alpha$, where $\alpha < \infty$. Since the iPC restricts energy injection, it can be demonstrated that this SEA system is dissipative and at least input-to-state stable [31]. Consider the user input $\dot{\theta}_L$ as well as the robot states θ_A and θ_L; input-to-state stability guarantees that as time increases, the states are bounded by some function of the input [32]. We can further show there always exists a set of E_U, E_L, and Z_d^* which ensures passivity; given a trajectory $\theta_L(t)$, the lower bound on physical interaction energy is directly correlated to E_L, so increasing E_L decreases α. In the worst case, iPCs bound the growth of SEA states; after sufficient tuning, iPCs assure passivity of the SEA interface.

Specifying iPC parameters Z_d^*, E_L, E_U, and the function f requires some degree of information about the target application; the SEA's compliance K, the desired impedance Z_d, and the anticipated range of interaction energies should be known. First, we choose a value of Z_d^* that can always be passively rendered—for the case of cascaded torque controllers, it has been shown that this condition is satisfied when rendering a pure stiffness less than or equal to K [17]. Moreover, because Z_d^* will be displayed near equilibrium, users should pick an acceptable impedance for small displacements during the given application. Next, we iteratively find the upper and lower limits of the interpolation region, where, as a rule of thumb, E_L and E_U are initialized at $1/4$ and $1/2$ of the anticipated maximum

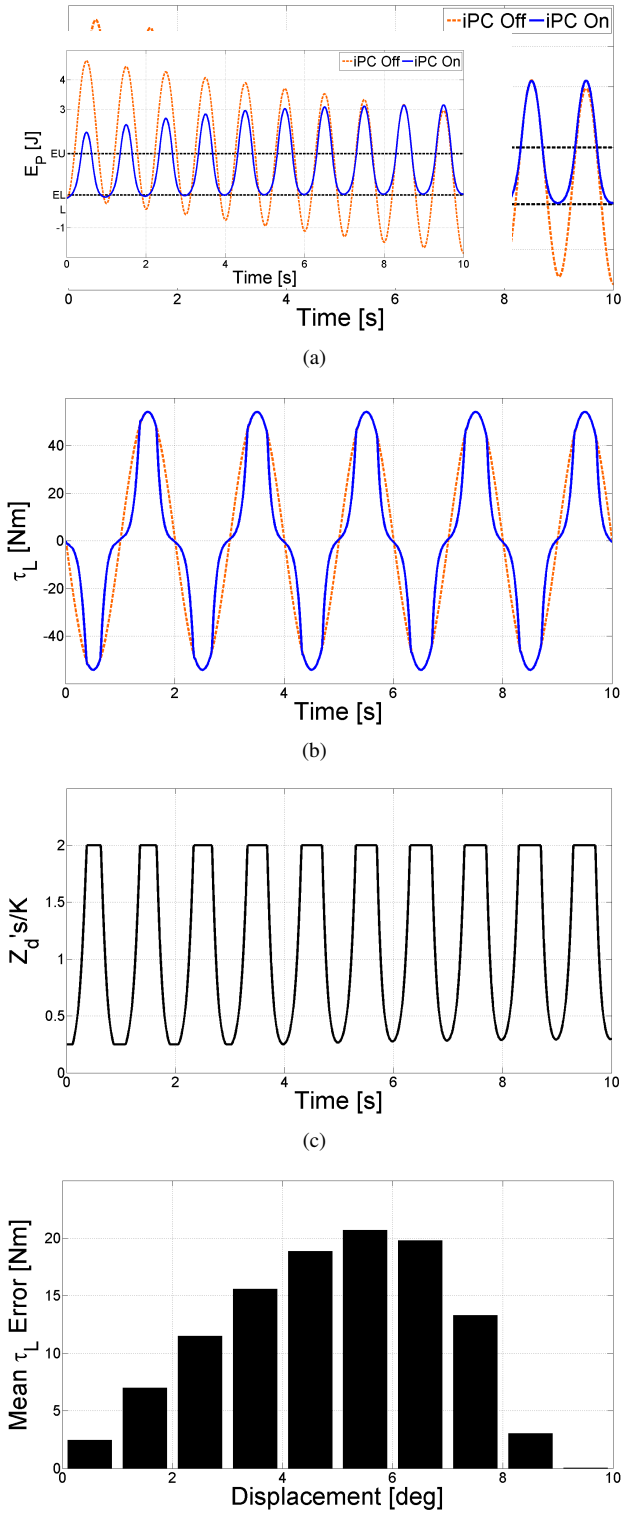

Fig. 5. Simulation of an SEA with our iPC. We attempt to render $Z_d s = 2K$ using cascaded torque-velocity control. Plant parameters are identical to those given for the flexion/extension knee joint of the LOPES [17], while controller gains match those enumerated by [9]. The human input is sinusoidal, oscillating spring output θ_L with 0.5 Hz frequency and 10° amplitude. No reference trajectory was provided, $\theta_{L,d} = 0$. (a) Interaction energy; horizontal lines mark lower ($E_L = 0.1$ J) and upper ($E_U = 1.5$ J) bounds of the iPC transition region. (b) Load torques. (c) iPC impedance; $Z_d^* s$ was initialized to $K/4$. (d) Load torques vs. spring displacement; each bar represents the mean difference between load torques with and without an iPC—shown in (b)—over 1° intervals of spring displacement.

This article has been accepted for publication in a future issue of this journal, but has not been fully edited. Content may change prior to final publication. Citation information: DOI 10.1109/TMECH.2016.2557727, IEEE/ASME Transactions on Mechatronics

energy, and then adjusted between trials based on resulting performance. Upper limit E_U must be less than the maximum energy, and lower limit E_L must be greater than zero. Finally, while other monotonic functions are viable, f was chosen to affect a linear interpolation between Z_d and Z_d^*, since this affords an intuitive interpretation of the impedance rendered throughout the transition region. So long as Z_d^* can always be rendered passively, the iPC guarantees at least input-to-state stability, regardless of the other parameter selections. To better demonstrate an SEA with iPC, example simulation results are provided in Fig. 5.

IV. Experimental Validation

We performed the subsequent experiments on a single degree-of-freedom linear SEA [33]. Our device—along with its enumerated components—is shown in Fig. 6. A brushed DC motor (Maxon Motor, RE 30) and rotary incremental encoder (Maxon Motor, HEDL 5540) are mounted to the ground frame; this motor drives a cable-wrapped pulley to control the translational slider's motion. An elastic element, which has been characterized to have stiffness $K = 1075$ N/m, lies between the slider and load and consists of a compactly-housed bidirectional spring together with a linear incremental encoder (US Digital, EM1-0-500-I) that directly measures spring deflection. Our experimental platform was designed for two load conditions: a fixed output for studying SEA force control, and a backdrivable mode for testing SEA interaction control. When varying load position, we employed another identical motor and transmission unit rigidly attached to the spring output. This second motor was treated as a pure velocity source, and resulting load positions were measured by subtracting spring deflection from actuator position. Controllers were executed using MATLAB/Simulink, and data acquisition at a sampling rate of 1 kHz was realized by QuaRC.

A. Demonstration of MRAC for SEAs

We here seek to experimentally verify that the proposed MRAC for SEAs can provide desired force performance despite errors in the initial parameter estimates. During this test we rigidly attached our linear SEA output to the ground frame such that x_L was fixed; accordingly, actuator translation directly corresponded to load forces, $F_L = Kx_A$. The system attempted to track a sinusoidal desired load force $F_{L,d}$ with 0.5 Hz frequency and an amplitude oscillating between ± 15 N—due to the proportionality of load force and actuator position, this equated to an appropriately scaled desired actuator trajectory $x_{A,d}$. In picking the second order transfer function for the reference model (6), we selected a natural frequency of 10 Hz and a critical damping ratio. Given that the resultant reference poles are twenty times faster than the signal frequency, $Q_f(s) \approx 1$, and the desired load force can be accurately output with low impedance (19).

Recall that the parameter vector ϕ contains estimates of J_A, B_A, K, μ_1, and μ_2. We purposely initialized ϕ to be different from ϕ^*, the "true" parameter values, to demonstrate that errors in $\hat{J}_A$, $\hat{B}_A$, $\hat{K}$, $\hat{\mu}_1$, and $\hat{\mu}_2$ can be accommodated under MRAC for SEAs. Practically, these intentional mistakes were meant to simulate a situation in which the plant had not been exactly identified, or where its properties had changed over time. The parameter estimate ϕ was updated in real time by integrating the adaption law (17). When constructing the control law (7), we determined the sign of velocity via continuous $sat(tanh(\cdot))$ functions for f_1 and f_2. The symmetric positive definite matrix P was chosen using the Kalman-Yakubovich lemma such that errors in actuator position were weighted significantly higher than errors in actuator velocity; moreover, the scalar gain γ was tuned so convergence could be observed over the test's 30 s length.

Fig. 7 depicts the results of this experiment, both in terms of actuator position and parameter estimates—these plots allow

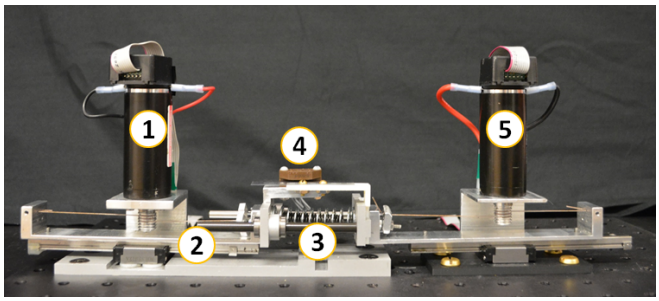

Fig. 6. Experimental linear SEA test-bed: (1) actuator-side DC motor, (2) translational slider, (3) bidirectional spring, (4) incremental encoder, (5) load-side DC motor.

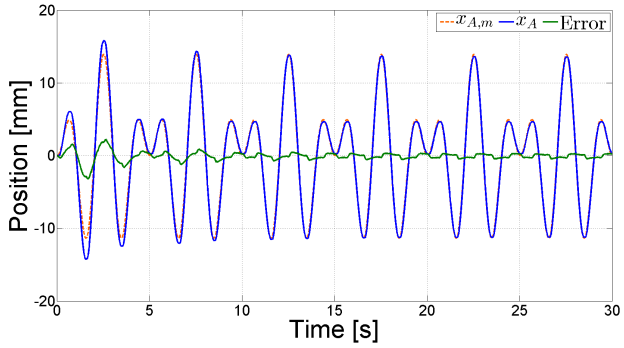

(a)

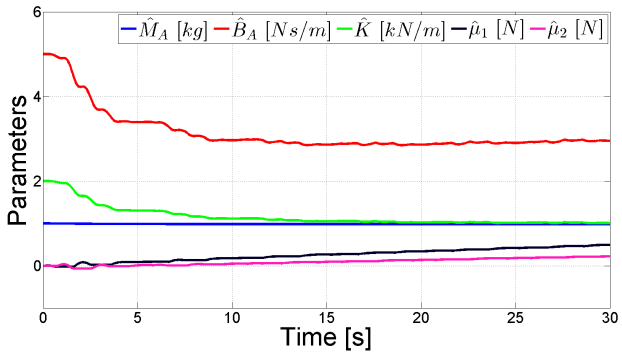

(b)

Fig. 7. Example force control performance using MRAC for SEAs. (a) Comparison of reference model and actuator position: error, which is defined as the difference between x_A and $x_{A,m}$, decreases in amplitude as x_A converges to $x_{A,m}$. (b) Parameter adaption for an unknown plant: the estimated plant parameters converge from erroneous initial conditions to yield desired closed-loop behavior. Prior to this test, we identified $M = 0.5$ kg, $B_A = 10$ N·s/m, and $K = 1075$ N/m.

This article has been accepted for publication in a future issue of this journal, but has not been fully edited. Content may change prior to final publication. Citation information: DOI 10.1109/TMECH.2016.2557727, IEEE/ASME Transactions on Mechatronics

us to evaluate MRAC stability and parameter convergence. From Fig. 7(a) it is evident that x_A more closely resembles $x_{A,m}$ as t increases; furthermore, performance improvements temporally correspond to the parameter adjustments. Position error does not converge to zero, however, which we believe stems from an unknown and repeated model variation, possibly motor backlash. Turning our attention to Fig. 7(b), we observe that the parameters desirably change so that F_A induces model following, but do not necessarily converge to their true values—e.g., $\hat{M}_A$ settles near $2M_A$. This behavior again aligns with previously stated theoretical expectations, particularly since the input signal is not persistently exciting. Although Coulomb friction parameters grew throughout the given time scale, they converged during longer tests.

B. Comparison of DOB and MRAC for SEAs

The following experiment endeavors to exhibit overarching stability and convergence trends for both robust and adaptive SEA force controllers, and focuses on the consequences of parameter uncertainty. Our goal here is not to claim one approach is "better," but rather to demonstrate that, unlike DOB methods, MRAC for SEAs is stable under arbitrary parameter uncertainty. We employed the robust controller described by [10]—which includes a filter $Q(s)$, a PD controller $C(s)$, and a nominal plant $P_n(s)$—together with our proposed MRAC for SEAs. The spring output was again rigidly attached to the ground frame, and each controller attempted to track a sinusoidal load force of 10 N amplitude and 0.5 Hz frequency for 10 s. Before performing any testing, we experimentally identified our SEA. The estimated plant parameters, along with reference model parameters, DOB control gains, and MRAC control gains, are enumerated in Table I. By inserting these values into the controller developed within Section II, as well as the DOB block diagram introduced in [10], the following experimental results can be replicated through simulation.

While we kept other initial parameters at their true value, we increased the estimated spring constant $\hat{K}$ by $0.5K$ after each pair of trials. Of course, changing $\hat{K}$ introduced parameter estimation error and provided a straightforward means to monitor the influence of system knowledge on controller behavior. A total of 8 trials were performed—4 with each controller—and the experimental results are plotted in Fig. 8. Norm position error here refers to the L_2-norm of the difference between x_A and $x_{A,m}$ taken over 2 s intervals. Note that the DOB method

TABLE I
PLANT PARAMETERS AND CONTROLLER GAINS

Plant $P_n(s)$		**Model** $Q(s)$	
M_A	0.5 kg	ω_n	10 Hz
B_A	10 N·s/m	ζ	1
K	1075 N/m		
$\mu_1,\ \mu_2$	0		
DOB Gains $C(s)$		**MRAC Gains**	
K_P	100 N/m	Q	$10^6(I_2)$
K_D	10 N·s/m	γ	10^4

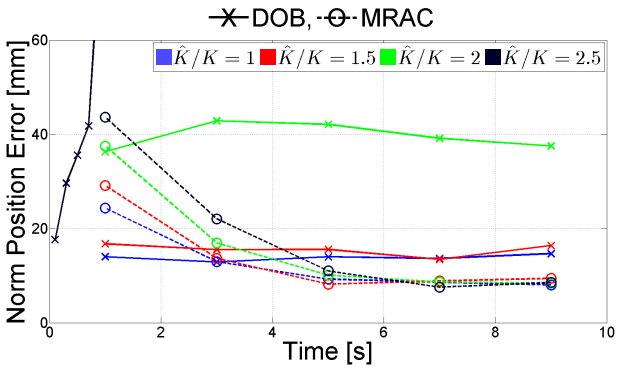

Fig. 8. Performance of DOB and MRAC during SEA force control while parameter estimation errors are present. When $\hat{K}/K = 2.5$ the DOB approach becomes rapidly unstable.

quickly becomes unstable when $\hat{K} = 2.5K$; hence, its norm position error is uniquely calculated at 0.2 s increments.

Two general trends can be extracted from Fig. 8: (a) the robust controller offered consistent performance throughout individual tests, while adaptive controller performance converged toward a common behavior, and (b) parameter uncertainty incurred instability in the robust controller, yet did not alter the long-term tracking of our adaptive controller. Increasing estimated parameter error augments the magnitude of a multiplicative perturbation Δ for DOB, but has no effect on Δ within MRAC; as shown, when $\Delta \to \infty$, DOB performance degrades ($\hat{K}/K = 2$) and eventually becomes unstable ($\hat{K}/K = 2.5$). The plot also suggests that MRACs provide better performance even in the absence of parameter error—potential gain variations and model inaccuracies, however, prevent us from inferring an underlying advantage.

C. Impact of iPC Settings on SEA Performance

We next endeavored to heuristically establish how different iPC parameter selections altered the behavior of an SEA under impedance control. During this test load position x_L was methodically varied by a second actuator, which attempted to follow a 0.5 Hz frequency and 4.25 mm amplitude cosine wave that had a -4.25 mm offset bias; simultaneously, our SEA interface sought to passively render $Z_d s = 2K$. We performed 9 trials, each 120 s in duration. With the intention of providing a consistent means for comparison, we first conducted a "baseline" case where the SEA used cascaded force control, the iPC upper energy bound E_U equaled 0.05 J, and the iPC passive impedance $Z_d^* s$ was defined as $0.1K$. Subsequent trials changed one parameter—whether that be the controller, E_U, or Z_d^*—with respect to this baseline case. Control gains, E_L, and other variables were held constant throughout.

Plots of averaged load force vs. load displacement are shown in Fig. 9. The slope of these curves corresponds to Zs, the stiffness rendered at the SEA output. Near low energy states the system renders stiffnesses less than $2K$; however, as displacement increases, stiffnesses approaching the desired $2K$ were observed during each trial. We found that smaller values of E_U and K_d^* yield worse performance around

This article has been accepted for publication in a future issue of this journal, but has not been fully edited. Content may change prior to final publication. Citation information: DOI 10.1109/TMECH.2016.2557727, IEEE/ASME Transactions on Mechatronics

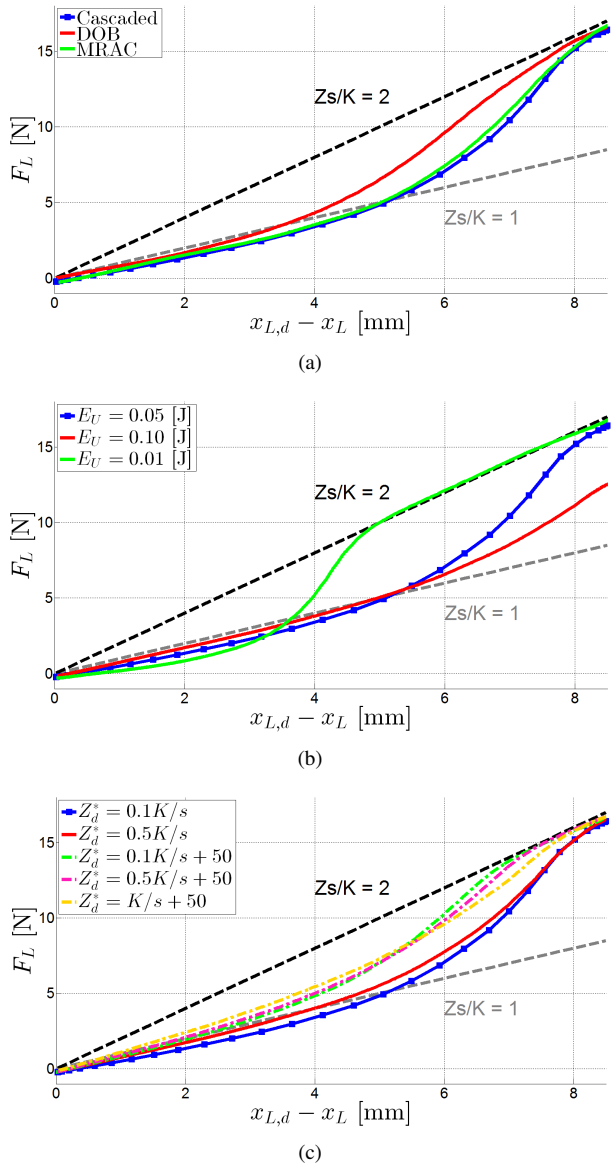

Fig. 9. Average load force as a function of load displacement while using different iPC parameter values. The baseline case, denoted by a blue line with square markers, is constant across each plot. Dashed gray and black lines correspond to the actual spring stiffness and desired output stiffness, respectively. (a) Application of different force control schemes. (b) Effects of varying the lower bound of the interpolation region. (c) Effects of varying the passive impedance; dashed colored lines indicate the addition of damping within Z_d^*.

equilibrium, but caused more rapid transitions to the desired stiffness. Increasing B_d^* enables higher perceived stiffnesses across the spectrum of displacement—since damping induces energy dissipation, this result matches expectation.

Numerical outcomes of Fig. 9 are summarized in Table II. Each row corresponds to a unique trial, while the first column denotes the modified parameter; tests should be contrasted with analogous trials—those varying the same parameter—as well as the baseline case. Let $\bar{x}_L$ indicate the mean load path across all trials; then x_L normalized error, a scaled metric of input deviation, was calculated as $\|x_L - \bar{x}_L\|/\|\bar{x}_L\|$. The amount of dissipated interaction energy was simply E_P measured at a trial's completion. The variable f is defined in (30), and dictates desired impedance. Perceived SEA stiffness

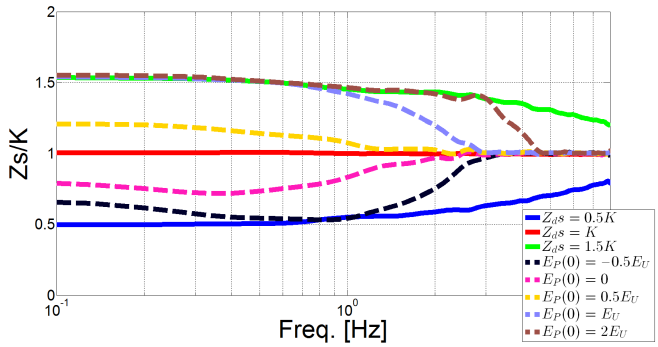

Fig. 10. Bode magnitude plot of normalized perceived stiffnesses for an SEA under impedance control. Cases without the iPC are shown in solid lines, while those with an iPC use dotted lines. Note that rendering $Z_d s = 1.5K$ without the iPC was not passive.

was computed according to $Zs = -F_L/x_L$, and singular data points where $x_L \to 0$ were discarded. Finally, recalling that $F_{L,d} = -Z_d x_L s$, load force normalized error was calculated as $\|F_L - F_{L,d}\|/\|F_{L,d}\|$.

Due to the presence of the proposed iPC, every listed trial maintained passivity throughout the experiment; in another novel result, the iPC worked successfully with linear, robust, and adaptive SEA force controllers. We found that increasing E_U unsurprisingly led to greater E_P—i.e., a more conservative system—but harmed other performance metrics. On the other hand, decreasing E_U instigated more aggressive behavior: E_P decreased, $Zs \geq 1.5K$ more often, and normalized F_L error diminished. Varying K_d^* produced a similar trade-off, where augmenting K_d^* reduced E_P but improved the remaining metrics; increasing the disparity between K_d and K_d^*, however, facilitated more accurate rendering during large x_L displacements at the expense of lower Z near equilibrium. The addition of B_d^* substantially increased both E_P and overall performance—but the use of B_d^* is sensitive to measurement delays and controller properties, and may not always be possible.

D. Effect of iPCs on SEA Bandwidth

In our final experiment, we studied the manner in which iPCs changed the high frequency behavior of impedance controlled SEAs. An actuator modulated load position such that x_L tracked a Schroeder multisine; this input had a flat frequency spectrum in the range $0.1-8$ Hz, and was scaled to a maximum amplitude of 5 mm. For the first 3 trials—performed without an iPC—the SEA attempted to render virtual stiffnesses $0.5K$, K, and $1.5K$. Throughout the next 5 trials—now including the iPC—the SEA sought to render $Z_d s = 1.5K$; here $Z_d^* s = 0.5K$, and only the initial interaction energy $E_P(0)$ varied between tests. A cascaded force controller was leveraged, along with iPC parameters given for the previous section's baseline case. We identified $Z(s)s$ by the MATLAB function `tfestimate` using measured input $-x_L$ and output F_L; all estimates had a coherence function above 0.9 across relevant frequencies.

The frequency responses of SEA virtual stiffness transfer functions are depicted in Fig. 10. For trials where $E_P(0) \geq 0$, the iPC maintained passivity, and for the test where $E_P(0) <$

This article has been accepted for publication in a future issue of this journal, but has not been fully edited. Content may change prior to final publication. Citation information: DOI 10.1109/TMECH.2016.2557727, IEEE/ASME Transactions on Mechatronics

TABLE II
EFFECT OF CONTROLLER, TRANSITION REGION, AND Z_d^* ON SEA PERFORMANCE WHILE $Z_d s = 2K$

	x_L Norm. Error	E_P Dissipated [J]	f Mean	f Std.	% Time $Zs \geq 1.5K$	F_L Norm. Error
Baseline	0.0136	0.0128	0.4768	0.3060	30.32	0.2905
DOB	0.0164	0.0157	0.3519	0.2830	40.35	0.2291
MRAC	0.0170	0.0154	0.4519	0.3061	32.61	0.2759
$E_U = 0.1$	0.0337	0.0354	0.5021	0.1853	15.77	0.3688
$E_U = 0.01$	0.0262	0.0008	0.4009	0.4264	52.11	0.1769
$Z_d^* = 0.5K/s$	0.0121	0.0068	0.5283	0.3398	32.59	0.2466
$Z_d^* = 0.1K/s + 50$	0.0184	0.0206	0.3265	0.2655	42.55	0.1771
$Z_d^* = 0.5K/s + 50$	0.0135	0.0166	0.3901	0.3010	42.37	0.1653
$Z_d^* = K/s + 50$	0.0131	0.0033	0.5160	0.3578	43.21	0.1515

0, the iPC dissipated energy. We conclude that—when using an iPC—the Bode magnitude plot of $Z(s)s$ is bounded by the frequency responses of strictly rendering $Z_d s$, the desired stiffness, and $Z_d^* s$, our secondary impedance. The iPC system displayed a range of stiffnesses between $Z_d s$ and $Z_d^* s$ at a given frequency; since Z_d' is dependent on E_P, this phenomenon stems from the time domain nature of our solution. Hypothetically, any behavior contained within the envelope described by $Z_d s$ and $Z_d^* s$ is therefore possible. We finally note that $Z(s)s$ converged to K as $\omega \to \infty$, demonstrating that the proposed iPC both works throughout a reasonable frequency range, and preserves underlying SEA high-frequency behavior.

V. DISCUSSION AND CONCLUSION

This article addressed compliant actuator control issues in the context of time domain theory, and focused on the fundamental tasks of stable SEA torque control and passive SEA impedance control. A model reference adaptive controller was first developed for SEAs, and was subsequently shown to track desired closed-loop behavior with Lyapunov stability. MRAC provides requested performance characteristics by continuously estimating the system's inertia, damping, spring stiffness, and Coulomb friction; we theoretically and experimentally demonstrated that our adaptive approach is stable despite parameter uncertainty, while state-of-the-art SEA disturbance observers may suffer parameter-induced instability. Moreover, unlike prior adaptive controllers for SEAs, the proposed formulation does not involve user dynamics, and can be safely integrated into an interaction control scheme using the described energy analysis method.

We next applied network theory—and, in particular, the time domain passivity approach—to ensure the safety of SEAs under impedance control schemes. Frequency domain tests such as the positive real property can determine linear controller passivity; however, each potential impedance/torque controller combination must be individually evaluated, and results cannot be extended to time-varying systems. On the other hand, by placing SEAs under impedance control in the context of network models, energy can be measured using passivity observers and dissipated through passivity controllers. We formulated the energy conditions for passivity when augmenting any stable torque controller with an arbitrary impedance, and developed a novel impedance passivity controller which enabled SEAs to passively render stiffnesses above their natural stiffness. It was interesting to note that compliant actuation necessarily introduces a mechanical time delay between commanded and actual end effector torque, which demands a different solution than the communication time delays common within haptic and bilateral teleoperation systems. Experiments highlighted the effects of the iPC transition region on performance metrics and the influences of an iPC on bandwidth.

Our methodical approach to compliant actuation under the lenses of time domain theory yielded a new torque control technique for this application, and more versatile impedance passivity assessments than were previously available. By means of these gains in compliant actuator control, we hope to increase the prevalence and effectiveness of elastic and safe manipulator designs for human-robot interaction. Although this work focused on SEAs—the most fundamental case of compliant actuation—many of the same concepts may be extended to variable stiffness actuators (VSAs), as well as other elastic actuator designs. Next steps involve incorporating our results within applications for compliant actuation, studying the potentially limiting properties of discrete time controller implementations, and more directly investigating VSAs while exploiting the proposed time domain techniques.

REFERENCES

[1] A. De Santis, B. Siciliano, A. De Luca, and A. Bicchi, "An atlas of physical human–robot interaction," *Mech. Mach. Theory*, vol. 43, no. 3, pp. 253–270, 2008.

[2] M. Zinn, O. Khatib, B. Roth, and J. K. Salisbury, "Playing it safe [human-friendly robots]," *IEEE Robot. Autom. Mag.*, vol. 11, no. 2, pp. 12–21, 2004.

[3] D. W. Robinson, "Design and analysis of series elasticity in closed-loop actuator force control," Ph.D. dissertation, Dept. Mech. Eng., MIT, Cambridge, MA, 2000.

[4] G. Pratt and M. M. Williamson, "Series elastic actuators," in *Proc. IEEE/RSJ Conf. Intelligent Robots Syst.*, vol. 1, 1995, pp. 399–406.

[5] J. F. Veneman, R. Ekkelenkamp, R. Kruidhof, F. C. van der Helm, and H. van der Kooij, "A series elastic- and bowden-cable-based actuation system for use as torque actuator in exoskeleton-type robots," *Int. J. Robot. Res.*, vol. 25, no. 3, pp. 261–281, 2006.

[6] J. S. Sulzer, R. A. Roiz, M. A. Peshkin, and J. L. Patton, "A highly backdrivable, lightweight knee actuator for investigating gait in stroke," *IEEE Trans. Robot.*, vol. 25, no. 3, pp. 539–548, 2009.

[7] G. A. Pratt, P. Willisson, C. Bolton, and A. Hofman, "Late motor processing in low-impedance robots: Impedance control of series-elastic actuators," in *Proc. American Control Conf.*, 2004, pp. 3245–3251.

[8] G. Wyeth, "Control issues for velocity sourced series elastic actuators," in *Proc. Australasian Conf. Robot. Autom.*, 2006.

[9] H. Vallery, R. Ekkelenkamp, H. Van Der Kooij, and M. Buss, "Passive and accurate torque control of series elastic actuators," in *Proc. IEEE/RSJ Conf. Intelligent Robots Syst.*, 2007, pp. 3534–3538.

[10] K. Kong, J. Bae, and M. Tomizuka, "Control of rotary series elastic actuator for ideal force-mode actuation in human–robot interaction applications," *IEEE/ASME Trans. Mechatronics*, vol. 14, no. 1, pp. 105–118, 2009.

[11] M. Grun, R. Muller, and U. Konigorski, "Model based control of series elastic actuators," in *Proc. IEEE RAS & EMBS Int. Conf. Biomed. Robot. Biomech.*, 2012, pp. 538–543.

[12] J. Bae, K. Kong, and M. Tomizuka, "Gait phase-based smoothed sliding mode control for a rotary series elastic actuator installed on the knee joint," in *Proc. American Control Conf.*, 2010, pp. 6030–6035.

[13] W. M. dos Santos and A. A. Siqueira, "Robust torque control based on $\mathcal{H}_\infty$ criterion of an active knee orthosis," in *Proc. IEEE RAS & EMBS Int. Conf. Biomed. Robot. Biomech.*, 2014, pp. 644–649.

[14] J. S. Mehling and M. K. O'Malley, "A model matching framework for the synthesis of series elastic actuator impedance control," in *Proc. Mediterranean Conf. Control Autom.*, 2014, pp. 249–254.

[15] B. J. Misgeld, A. Pomprapa, and S. Leonhardt, "Robust control of compliant actuators using positive real $\mathcal{H}_2$-controller synthesis," in *Proc. American Control Conf.*, 2014, pp. 5477–5483.

[16] A. Calanca and P. Fiorini, "Human-adaptive control of series elastic actuators," *Robotica*, vol. 32, no. 8, pp. 1301–1316, 2014.

[17] H. Vallery, J. Veneman, E. Van Asseldonk, R. Ekkelenkamp, M. Buss, and H. Van Der Kooij, "Compliant actuation of rehabilitation robots," *IEEE Robot. Autom. Mag.*, vol. 15, no. 3, pp. 60–69, 2008.

[18] N. L. Tagliamonte and D. Accoto, "Passivity constraints for the impedance control of series elastic actuators," *Proc. I. Mech. Eng. I-J Sys.*, vol. 228, no. 3, pp. 138–153, 2014.

[19] M. Mosadeghzad, G. Medrano-Cerda, J. Saglia, N. G. Tsagarakis, D. G. Caldwell *et al.*, "Comparison of various active impedance control approaches, modeling, implementation, passivity, stability and trade-offs," in *Proc. IEEE/ASME Conf. Adv. Intelligent Mechatronics*, 2012, pp. 342–348.

[20] F. Sergi and M. K. O'Malley, "On the stability and accuracy of high stiffness rendering in non-backdrivable actuators through series elasticity," *Mechatronics*, vol. 26, pp. 64–75, 2015.

[21] S. Ulrich, J. Z. Sasiadek, and I. Barkana, "Modeling and direct adaptive control of a flexible-joint manipulator," *J. Guid. Control Dynam.*, vol. 35, no. 1, pp. 25–39, 2012.

[22] I. Barkana, "Simple adaptive control—a stable direct model reference adaptive control methodology—brief survey," *Int. J. Adapt. Control*, vol. 28, no. 7-8, pp. 567–603, 2014.

[23] B. Hannaford and J.-H. Ryu, "Time-domain passivity control of haptic interfaces," *IEEE Trans. Robot. Autom.*, vol. 18, no. 1, pp. 1–10, 2002.

[24] F. Ferraguti, C. Secchi, and C. Fantuzzi, "A tank-based approach to impedance control with variable stiffness." in *Proc. IEEE Conf. Robot. Autom.*, 2013, pp. 4948–4953.

[25] K. J. Åström and B. Wittenmark, *Adaptive Control*, 2nd ed. Mineola, NY, USA: Dover Publications, 2008.

[26] P. A. Ioannou and J. Sun, *Robust Adaptive Control*. Mineola, NY, USA: Dover Publications, 2012.

[27] N. Hogan, "Impedance control: An approach to manipulation," *J. Dyn. Syst. Meas. Control*, vol. 107, no. 1, pp. 1–24, 1985.

[28] J. E. Colgate and N. Hogan, "Robust control of dynamically interacting systems," *Int. J. Control*, vol. 48, no. 1, pp. 65–88, 1988.

[29] R. J. Adams and B. Hannaford, "Stable haptic interaction with virtual environments," *IEEE Trans. Robot. Autom.*, vol. 15, no. 3, pp. 465–474, 1999.

[30] P. F. Hokayem and M. W. Spong, "Bilateral teleoperation: An historical survey," *Automatica*, vol. 42, no. 12, pp. 2035–2057, 2006.

[31] A. Jafari and J.-H. Ryu, "Input-to-state stable approach to release the conservatism of passivity-based stable haptic interaction," in *Proc. IEEE Conf. Robot. Autom.*, 2015, pp. 285–290.

[32] H. K. Khalil and J. Grizzle, *Nonlinear Systems*. Upper Saddle River, NJ, USA: Prentice Hall, 2002, vol. 3.

[33] F. Sergi, M. M. Lee, and M. K. O'Malley, "Design of a series elastic actuator for a compliant parallel wrist rehabilitation robot," in *Proc. IEEE Conf. Rehab. Robot.*, 2013.

Dylan P. Losey (S'14) received the B.S. degree in mechanical engineering from Vanderbilt University, Nashville, TN, USA, in 2014. Since then, he has been working toward the Ph.D. degree in mechanical engineering at Rice University, Houston, TX, USA, as a member of the Mechatronics and Haptic Interfaces Laboratory. His research interests include human-robot interaction and machine learning. Mr. Losey received an NSF Graduate Research Fellowship in 2014.

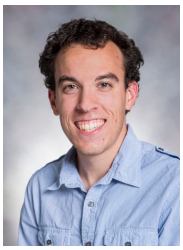

Andrew Erwin (S'12) received the B.S. degree in mechanical engineering from the University of Massachusetts, Amherst, MA, USA, in 2012, and the M.S. degree in mechanical engineering from Rice University, Houston, TX, USA, in 2014. Supported by an NSF Graduate Research Fellowship, he is currently working toward the Ph.D. degree at the Rice University Mechanical Engineering Department as a member of the Mechatronics and Haptic Interfaces Laboratory. His research interests include haptics, MR-compatible robotics, and series elastic actuators.

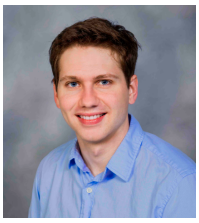

Craig G. McDonald (S'14) received the B.S.E. degree in Mechanical Engineering and Applied Mechanics from the University of Pennsylvania, Philadelphia, PA, in 2012. He is currently working toward the Ph.D. degree in Mechanical Engineering at Rice University, Houston, TX, as a member of the Mechatronics and Haptics Interfaces Laboratory. He is a trainee of the Rice University/Baylor College of Medicine Neuroengineering IGERT program, funded by the NSF. His research interests include robotic exoskeletons and haptic interfaces, robotic manipulation, and machine learning.

Fabrizio Sergi (M'13) is Assistant Professor of Biomedical Engineering at the University of Delaware, where he directs the Human Robotics Lab. At the University of Delaware, he holds affiliated appointments in the Mechanical Engineering Department and in the Biomechanics and Movement Science Program. He was previously a Research Scientist and Post-doctoral fellow in the Mechanical Engineering Department at Rice University, following his B.S, M.S. and Ph.D. degrees in biomedical engineering from Università Campus Bio-Medico di Roma, Rome, Italy, in 2005, 2007 and 2011, respectively. His research interests include wearable robotics, robot-aided neurorehabilitation, and the analysis of robot-assisted motor learning. He is member of the IEEE, of the IEEE RAS and EMBS societies, and of the ASME.

Marcia K. O'Malley (SM'13) received the B.S. degree from Purdue University, West Lafayette, IN, USA, in 1996, and the M.S. and Ph.D. degrees from Vanderbilt University, Nashville, TN, USA, in 1999 and 2001, respectively, all in mechanical engineering. She is currently a Professor of mechanical engineering and computer science with Rice University, Houston, TX, USA, and directs the Mechatronics and Haptic Interfaces Laboratory. She is a Fellow of the American Society of Mechanical Engineers and serves as an Associate Editor for the ASME Journal of Mechanisms and Robotics.